EUROPEAN COMMISSION

HORIZON 2020 PROGRAMME
TOPIC H2020-LCE-07-2016-2017
Developing the next generation technologies of renewable electricity and heating/cooling

GA No. 727523

Next – generation interdigitated back-contacted silicon heterojunction solar cells and modules by design and process innovations

NextBase - Deliverable report

T8.1 Assessment of loss mechanisms in IBC-SHJ devices

Deliverable No.	NextBase D8.1	
Related WP	8	
Deliverable Title	Report on the breakdown of optical and electrical losses in IBC-SHJ solar cells and optimization strategies	
Deliverable Date	30 September 2017	
Deliverable Type	REPORT	
Dissemination level	Public	
Author(s)	Lars Korte, Christoph Stang (HZB)	22-9-2017
Checked by	Lars Korte (HZB)	23-09-2017
Reviewed by (if applicable)	Paul Procel, Olindo Isabella (TUD), Kaining Ding (Jülich)	26-09-2017
Approved by	Kaining Ding	27-09-2017
Status	Final/Submitted	28-09-2017

Disclaimer/ Acknowledgment

This project has received funding from the European Union's Horizon 2020 research and innovation programme under grant agreement No 727523. The information and views set out in this publication does not necessarily reflect the official opinion of the European Commission. Neither the European Union institutions and bodies nor any person acting on their behalf, may be held responsible for the use which may be made of the information contained therein.

Publishable summary

In order to investigate the efficiency potential and the optical and electrical losses in interdigitated rear-contact silicon heterojunction (IBC-SHJ) solar cells, 2D-simulation studies of the electrical and optical properties of such cells were carried out using the numerical device simulator Sentaurus TCAD.

Some quite general conclusions could be drawn from the simulations:

- As long as the passivation properties of different films (emitter / back surface field (BSF)) are at the same level, the ratio of emitter-vs-BSF coverage, and the absolute size of the contacts as defined by this ratio and the unit cell pitch, have a negligible influence on the open circuit voltage
- The fill factor, on the other hand, is very sensitive to the contact size
- due to the high resistivity of a-Si:H, a larger contact is generally beneficial for current collection, which leads to higher fill factors (FFs)
- The best pitch is mostly influenced by gap size, minority carrier diffusion length and base resistivity: too large pitches, above the minority carrier diffusion length, lead to current collection losses (drop in photocurrent, j_{sc}) as well as increasing series resistance (FF drop), while the limitations towards small pitches are mostly determined by the structure sizes that can be realized technologically
- For the simulated (realistic) materials properties, the optimum for the technological pitch is of the order of 0.5-1.5 mm.
- The best emitter/BSF ratio is decided by the current collection probability (determined by c-Si bulk and surface properties) as well as the a-Si:H quality (conductivity, contact resistance); with realistic properties of the contact materials it is roughly emitter/BSF = 80/20.
- Both emitter and BSF should be covered as thoroughly as possible by metal contacts; metallization gaps of only 50 µm, which are at the lower end of technologically relevant gap widths, already lead to a slight decrease in solar cell fill factor (a few tenths of a % abs.).
- Regarding optical properties, it could be demonstrated that the front side antireflection/light trapping structures currently available within NextBase are on par with those of the current world record IBC-SHJ cell, which account for ~1 mA/cm² photocurrent loss as compared to the maximally available 43.2 mA/cm² from c-Si wafers, or ~2.3%rel..

Further planned investigations will rely on a fully integrated combination of optical and electrical simulations in one accurately modelled structure, which allows distinguishing between many distinct loss contributions both on the optical as well as on the electrical side. With this “simulation toolbox” in place, we are able to make quantitative assessments and optimizations more specifically for the different structures investigated by the partners. The data necessary to calibrate the model to the different partners’ IBC structures is currently being collected.

Contents

1 Introduction 6
1.1 Background & aim of the deliverable 6
1.2 Simulation approach 6
2 Results 8
2.1.1 Efficiency potential of interdigitated back contact SHJ solar cells 8
2.1.2 Fully integrated electrical & optical loss analysis 9
2.1.3 Contact geometry 11
2.1.4 Optimisation of the TCO/emitter and TCO/BSF interfaces 14
3 Risks and interconnections 16
3.1 Risks/problems encountered 16
3.2 Interconnections with other deliverables 16
4 Conclusion/summary 17
5 Literature 18

List of acronyms, abbreviations and definitions

Table 0.1 Acronym table

Abbreviation	Explanation
IBC	Interdigitated back contact (solar cell)
SHJ	Silicon heterojunction (solar cell)
a-Si:H	Hydrogenated amorphous silicon
BSF	Back surface field
TCO	Transparent conductive oxide
Voc	Open circuit Voltage
jsc	Short circuit current density
FF	Fill factor
η	Power conversion efficiency

1 Introduction

1.1 Background & aim of the deliverable

Simulation and modelling are valuable tools for the investigation of solar cells to gain insights into loss mechanisms and identify routes for potential device optimisation. Within NextBase, the aim of advanced 1-3D numerical modelling is to carry out quantitative and predictive simulations that can provide insight into the reasons for losses in the devices processed in the project (mostly WP5) (→ MS6). Furthermore, sensitivity analyses shall be carried out to identify those materials properties that are critical for ultimately reaching high efficiencies. Ultimately, a pathway will be described to reach the efficiencies defined in the project goals, and beyond (D8.4).
As a first step to these goals, in the present deliverable we have thoroughly analysed the existing IBC-SHJ solar cell concepts both by electrical and optical simulations powered by Sentaurus TCAD.

1.2 Simulation approach

The solar cell devices are represented by a 2D unit cell designed using the corresponding real device geometry and layer stacks. A typical device geometry is shown in **Figure 1**:

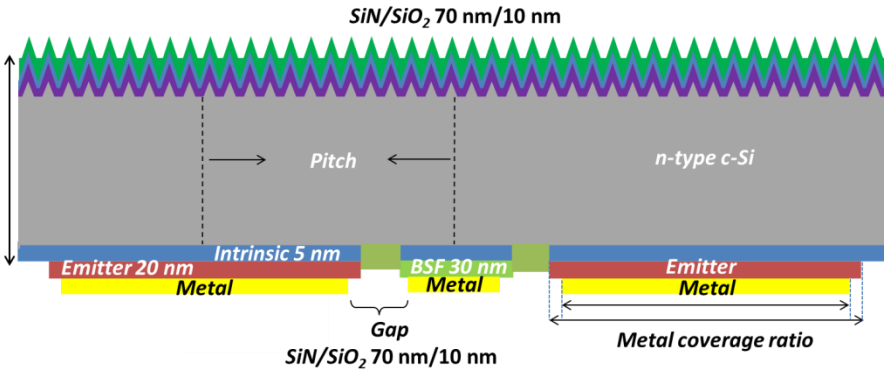

Figure 1: *Typical geometry, front- and rear side layer stacks of an interdigitated back contact silicon heterojunction solar cell (side view).*

On the rear side, the cell consists of alternating stripes of emitter and BSF strips (in **Figure 1**, these consist of (p/i) and (n/i) layer stacks, respectively), which are contacted either with direct metallizations, as shown here, or with metal/TCO stacks. The coverage of emitter and BSF regions with these contact stacks is a free parameter which has a huge influence on the device performance (cf. sec. 2.4.1). In **Figure 1**, an additional gap region is sketched which is sometimes used to isolate the p- and n-contact regions from each other. Alternatively, the emitter and BSF regions can be overlapping. In order to reduce computational cost, the repeating stripe pattern of the IBC is usually described as a repetition of a smallest possible domain, a so-called unit cell, as designated by the dashed lines in **Figure 1**. Thus, in the basic unit cell there is half a single emitter contact (p+ doped region) and half a base contact (n+ doped region), which are then mirrored along the dashed lines. Note, that this means, that *this "computational pitch" is only half as long as the commonly used definition (termed*

"technological pitch" in the following), which is based on translational symmetry (e.g. from the center of the emitter stripe to the center of the next emitter stripe).
To simulate the properties of a solar cell, conventionally two different simulation domains are introduced: an optical one that creates a charge carrier generation profile by taking into account the device's geometry including its usually textured surface; and an electrical one, based on a drift-diffusion model, where textured or structured surfaces are usually avoided. The generation profile of the optical model is then simply applied to the electrical domain leading to a loss in simulation accuracy as for instance the impact of the textured surface on the electrical properties of the device cannot be accounted for.
In contrast to this simplified approach, **TUD** developed a Sentaurus TCAD-based opto-electrical model, which involves a two dimensional geometry including the exact modelling of a pseudo-random pyramids front texturing morphology both in the optical and electrical simulations. Reflectance, transmittance, internal and external quantum efficiency measurements are then used to calibrate the model, as shown in [Procel2017] for IBC-polySi devices. The **TUD** approach was used in sections 2.1.2 and 2.1.4.

In simulations that mainly focus on the electrical properties of the device, on its rear side in particular, the conventional approach of a planar device and an externally created generation profile is used (sections 2.1.1 and 2.1.3).

2 Results

2.1.1 Efficiency potential of interdigitated back contact SHJ solar cells

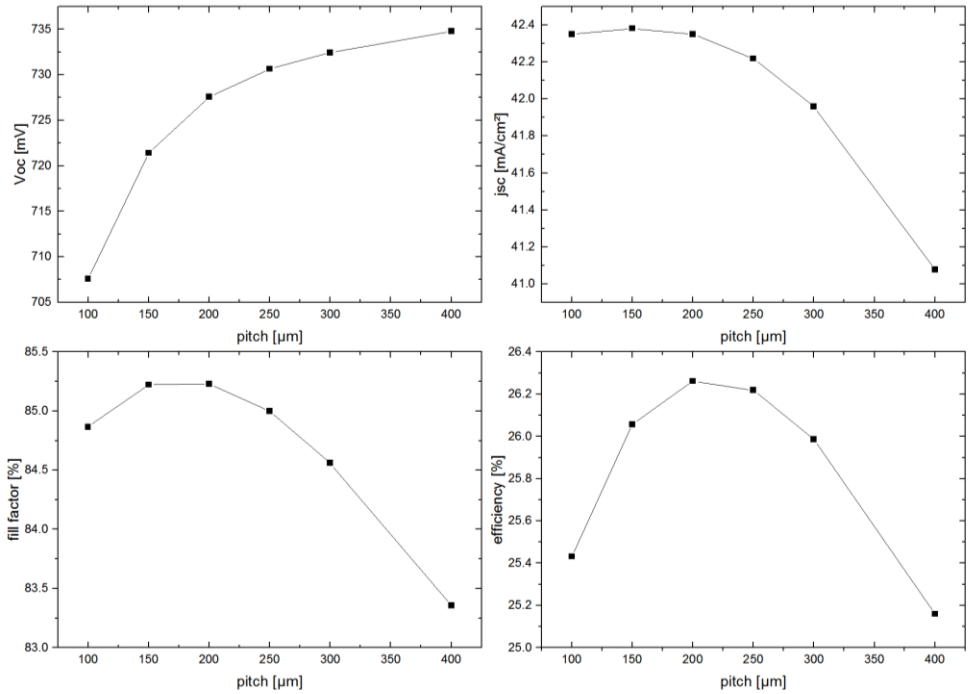

Figure 2: *Simulated solar cell parameters for an idealized (n)c-Si based IBC-SHJ cell without parasitic optical absorption and negligible bulk and volume recombination losses.*

In order to obtain benchmark values for the ultimate efficiency potential of interdigitated back contact cells, an idealized model was set up based on the following parametrizations:

- the wafer is n-type doped at 2Ωcm, and 150µm thick.
- the contacts and all other surfaces are replaced by an effective surface recombination velocity $S_{front} = S_{rear} = S_{c,base} = 0$ as a boundary condition. This yields a carrier lifetime of >15ms
- the emitter stripe half width is kept constant at 30 µm
- bulk recombination is limited by intrinsic mechanisms (Auger and radiative recombination), using Richter's parameterization [Richter2012]
- the textured front side is replaced by a flat polished surface with total optical transmission (T=100%) and considering simultaneously a modified AM1.5G spectral irradiance $S_{1-R} = S(\lambda)\times(1-R(\lambda))$ as incident light, where $S(\lambda)$ is the spectral irradiance of the standard AM1.5G spectrum and $R(\lambda)$ is the measured reflectance of an IBC precursor. Additionally, internal reflectances of the front and rear surfaces of 100% are introduced in the simulations. Thus, the overall power distribution between reflected and absorbed light is based on an experimental result, and parasitic absorption in the passivation, ARC and contact layers is calculated based on the refractive indices of the films.

Figure 2 shows solar cell parameters simulated under these assumptions, where the contact pitch ("computational pitch", c.f. above) is considered as the free parameter. The maximum of the efficiency is given by the trade-off of j_{sc} and FF drop at large pitches, and drop of Voc and FF for small pitches.

These effects can be explained as follows: In IBC-SHJ cells, minority carriers travel to the p-n junctions via diffusive transport. Therefore, the bulk diffusion length of minority charge carriers is a key parameter for solar cell performance, and for too large pitches, an increasing fraction of the photogenerated minority charge carriers can't reach the emitter, decreasing j_{sc}. Furthermore, the base resistance of the wafer increases R_s for large pitches, leading to a decrease in FF. For small pitches, the recombination at the emitter regions decreases V_{oc} and FF, because the relative areal fraction of the emitter (with fixed width) increases for decreasing pitch.

The best cell, with a pitch of 200µm (thus, "technological" pitch 400µm), has a V_{oc} of 728 mV, j_{sc} 42.4mA/cm², fill factor of 85.2% and efficiency of 26.3%. Note, that this simulated efficiency result closely matches the experimental efficiency of the current record cell for this device structure (26.3% reported in [Yoshikawa2017] – 26.6% certified by NREL), however with deviations in fill factor (experimental in [Yoshikawa2017]: 83.8%) and V_{oc} (exp.: 744 mV), while the j_{sc} is also a close match to the experiment (42.3 mA/cm²). Since the experimental reflectance of our IBC cell precursor with excellent light trapping was used as an input, the matching j_{sc} essentially confirms that we are already able to realize experimentally similarly good optical properties as in the world record cell. Regarding the other deviations between simulation and experiment, it is probable that the higher V_{oc} is due to the lower wafer doping (3 Ωcm) of the wafer in Kaneka's record cell; part of the lower FF in the experimental cell could also be caused by the thus higher series resistance, as well as by other series resistance contributions e.g. in the metallization.

2.1.2 Fully integrated electrical & optical loss analysis

As mentioned in the introduction, ultimately an integrated simulation considering both the full optics and electrics of the IBC SHJ devices shall be carried out in NextBase (→ MS 6). Currently, the simulations developed by **TUD** to this end [Ingenito2014, Ingenito2015] are being adapted to silicon heterojunction devices. In the following, we present the potential of these simulations using the example of polycrystalline Si/SiO2 tunnel contacts [P. Procel et al., to be presented at EUPVSEC 2017].

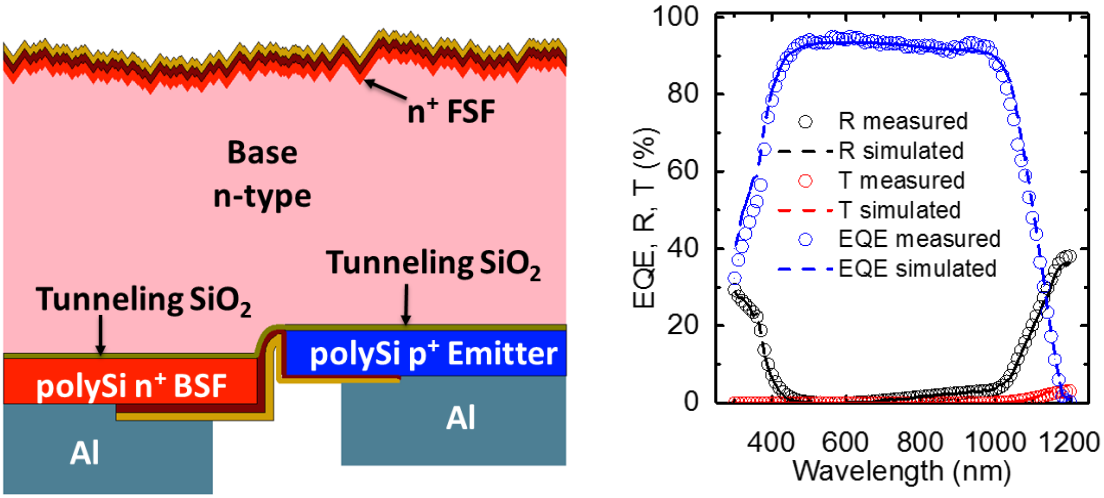

Figure 3: Sketch of the simulated IBC device structure with polycrystalline Si/SiO_2 tunnel contacts (left) and validation of the optical model by comparison to experimental results.

In Figure 3 the device structure is depicted. The model is parametrized using accurate inputs regarding the layer and contact stack properties, and calibrated by reflectance, transmission and IQE/EQE measurements. Figure 3 (right) shows an excellent agreement between the optical part of the calibrated simulation and previously published experimental reflection, transmission and quantum efficiency data [Yang2016]. The electrical parameters show a similarly good agreement, cf.

	J_{sc} (mA/cm^2)	V_{oc} (mV)	FF (%)	η (%)
Measured [Yang2016]	39.2	692	78.3	21.2
Simulated	39.5	691	78.4	21.4

Table 2. The model can thus be considered validated and calibrated for this specific device layout.

	J_{sc} (mA/cm^2)	V_{oc} (mV)	FF (%)	η (%)
Measured [Yang2016]	39.2	692	78.3	21.2
Simulated	39.5	691	78.4	21.4

Table 2: comparison of the electrical parameters extracted from the simulation with experimental results.

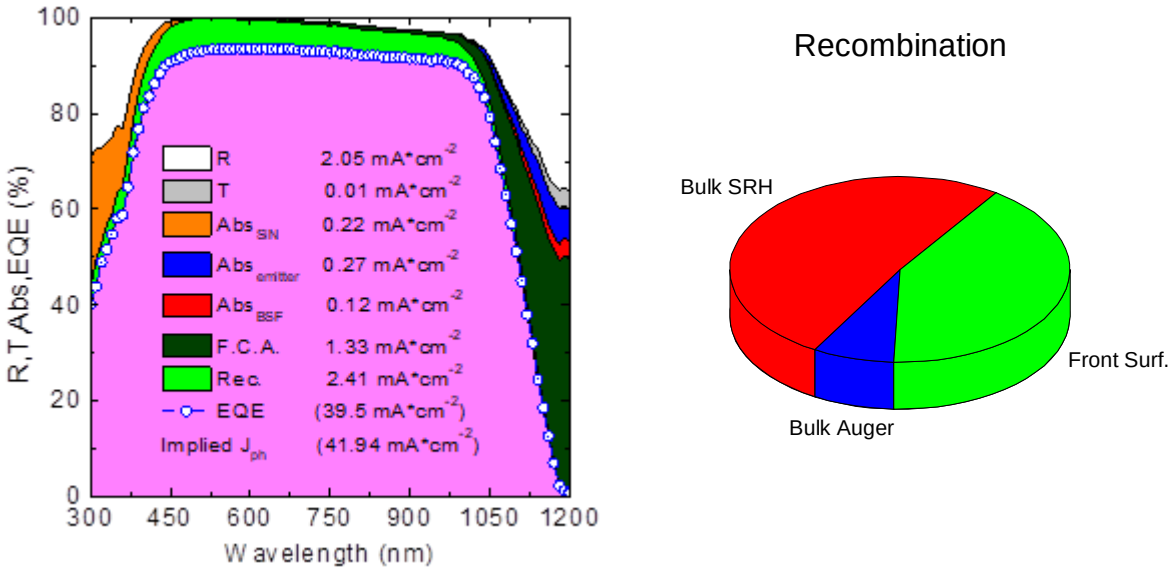

Figure 4: Wavelength dependence of optical reflection, transmission and absorption as well as electrical losses (recombination - "Rec.") for the IBC cell depicted in the previous figure, including experimental EQE data (circles) (left). Breakdown of the recombination losses into c-Si bulk defect- and Auger recombination as well as recombination at the front surface field (right).

Based on this calibrated model, Figure 4 demonstrates the potential of the simulation based approach j_{sc} analysis. The entire IQE or EQE curve can be decoded with regards to the different loss mechanisms. Especially the possibility to differentiate between absorption and recombination losses at the front as well as between free carrier absorption in the TCO and absorption in the emitter/BSF layers at the rear side allows for the specific optimisation of real devices.

It is worth noting that all loss mechanisms can be calculated for different solar cell conditions (i.e. at j_{sc}, maximum power point and V_{oc}), yielding input for further optimization of the devices.

2.1.3 Contact geometry

With both contacts of IBC solar cells on the same side, the total contact area is – in comparison to standard double-sided SHJ cells – essentially reduced by 50 %, which leads to an inherent increase in contact resistance. To mitigate this negative effect, a proper contact geometry must be designed and, most importantly, also manufactured. Interdigitated finger structures consisting of p- respectively n-type amorphous or nanocrystalline silicon represent the dominant concept among all project partners. This kind of geometry can be easily modelled and optimised in a 2D simulation environment, with relatively few key parameters: the width of the p- and the n-fingers, whose sum (including overlaps or gaps, cf. **Figure 1**) results in the pitch and the width of the metallisation for each finger. The accuracy of the manufacturing process determines the boundaries for the dimensions of these parameters. With photolithography based processes, very narrow metallisation gaps and very thin finger widths and sharp edges can be achieved, but wet chemical etching techniques might make overlapping of n- and p-layers necessary, in order to protect the underlying intrinsic amorphous silicon. With shadow mask based approaches the less optimal thickness profile of the n- or p-fingers leads to larger metallisation gaps, to guarantee a minimum thickness of the emitter/BSF layers below the TCO/metal. The simulation results are also influenced by various other parameters, most notably the thickness of the wafer, its specific resistivity and bulk lifetime, the contact resistivity of both contacts and the front side passivation.

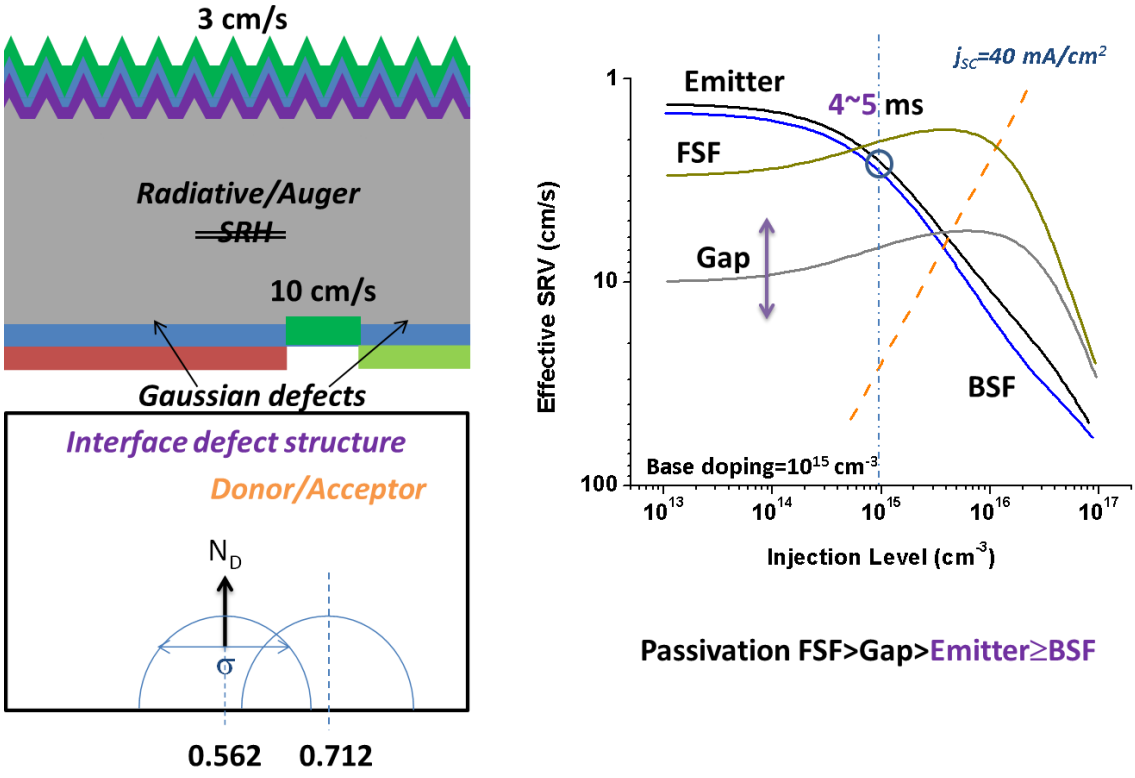

Figure 5: Sketch of the simulated IBC SHJ unit cell depicting schematically the Gaussian defect distribution assumed at the emitter and BSF heterointerfaces (left) and influence of this defect distribution on the injection level dependent effective

surface recombination velocities at these interfaces (right). For comparison, these dependencies are also shown for the front side and gap passivation, where a constant S was assumed.

Therefore, a first study was carried out on the influence of different passivation qualities in the emitter, BSF and gap regions. (n)c-Si with 270 µm thickness and a doping of 10^{15}/cm³ was assumed. Special effort was dedicated to realistic parametrization of the a-Si:H films in the emitter and BSF regions (Figure 5): (p) and (n)-type a-Si:H films were processed at **HZB** and characterized using photoelectron spectroscopy, yielding work functions of 5.17 and 4.14 eV, respectively, for the p- and n-type films as well as estimates for the gap defect state densities. When these parameters are included in a heterojunction model, they give injection-level dependent effective surface recombination velocities that differ considerably from those for constant *S*, as assumed for the cell's front and gap passivation. For the parameter set used here, the emitter passivation turned out to be slightly better than that of the BSF (lower effective recombination velocity S_{eff}). Interestingly, in the cell results simulated at **HZB**, Figure 6, the V_{oc} still increases slightly with increasing emitter fraction. However, this effect is rather marginal: Clearly, the change of efficiency with changing emitter-to-BSF ratio is dominated by the changes in fill factor. The fill factor peaks at an emitter-to-BSF ratio of 80/20; deviations of this value lead to increased losses due to electrical shading or, for too thin contact regions, due to a strongly increasing series resistance at the contact (a-Si:H bulk resistance + TCO/a-Si:H contact resistance).

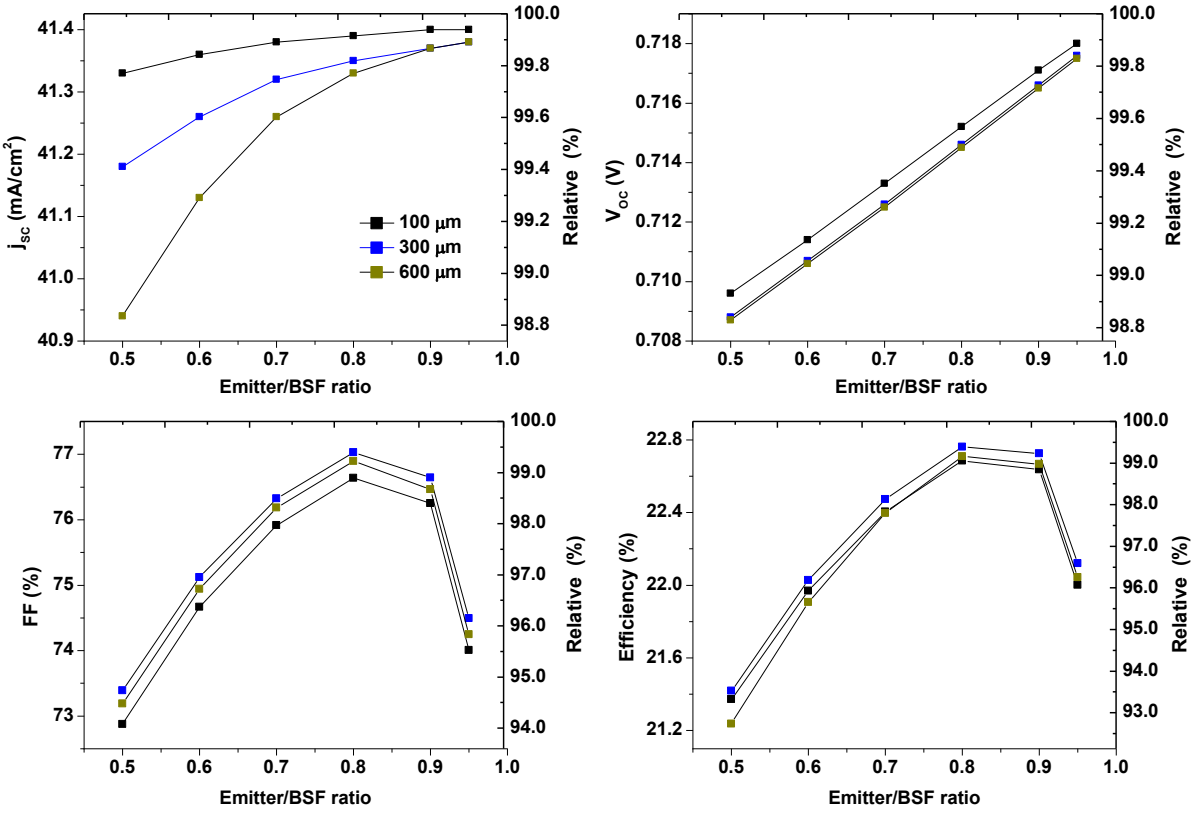

Figure 6: Solar cell parameters extracted from simulated illuminated I-V curves for the structure depicted in the previous figure, with varying emitter-to-BSF ratio. Gap width was fixed at 10µm, computational pitch 100/300/600 µm (thus, "technological" pitch 200/600/1200µm).

This was further investigated, considering an updated set of input parameters for the films and additionally a change from the depicted geometry with a passivated gap to a structure with overlapping n- and p-regions. The simulation results depicted in Figure 7 assume a wafer thickness of 260 µm, a specific resistivity of 3 Ωcm, a bulk lifetime of 10 ms and a well passivated front side (SRV_front = 5 cm/s). In contrast to the previous simulations, an overlap with a width of 15 µm of the p- and the n-regions was assumed as well as an asymmetrical metallisation gap of 40 µm (5 µm unmetallised p-region, 35 µm non-metallised overlap respectively n-region). These values correspond to the IBC-SHJ cells currently built at HZB (using photolithography). The study shown in Figure 7 (left) suggests, with these updated material and geometry parameters, a wider optimal emitter finger width of 1 to 2 mm while the BSF finger should be considerably thinner. Note, that the emitter and BSF widths given in in Fig. 7 are already the "technological" ones.

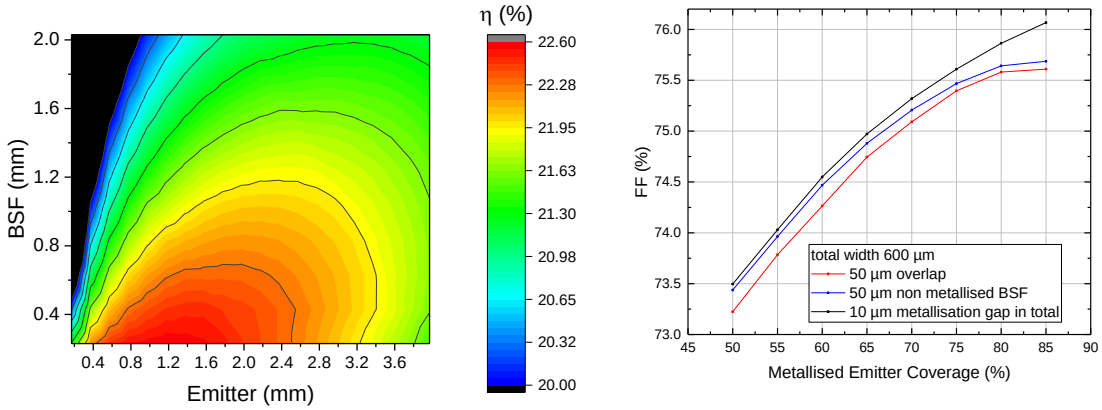

Figure 7: Simulated solar cell efficiencies for varying emitter and BSF strip widths (left), and dependence of the IBC-SHJ fill factor on the metallized emitter coverage, for three different contact geometries (see text).

The simulation study in Figure 7 (right) visualises the influence of emitter metallisation coverage on the FF. Since the p-amorphous layer itself is not very conductive, minority charge carriers will travel through the wafer until they reach the metallised part of the emitter region, where they are then collected. The black curve (symmetrical metallisation gap of 10 µm) represents the ideal case, in which increasing the metallised emitter coverage (mec) should always be beneficial until a too narrow BSF contact becomes limiting. This starts to happen at a mec value of 80 % if a more realistic metallisation gap of 50 µm is introduced only on the n-finger side (blue curve). The FF values reach a plateau. Having an overlap of p- and n-regions (red curve) instead of a simply non-metallised n-region (keeping the total width constant) does not change the overall trend, but has a slight detrimental effect on the FF regardless of metallised emitter coverage.

2.1.4 Optimisation of the TCO/emitter and TCO/BSF interfaces

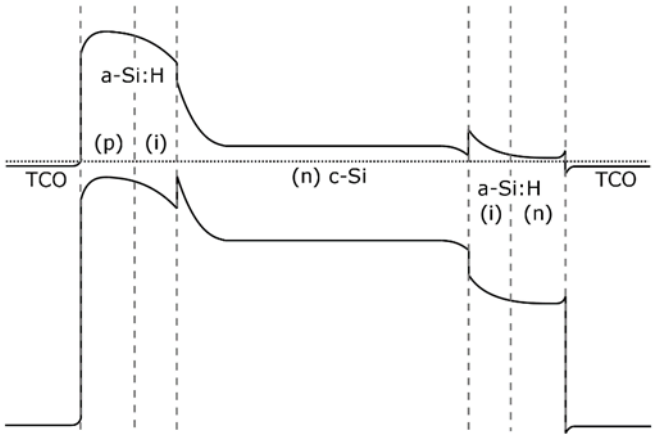

Figure 8: *Band diagram (schematic) of a silicon heterojunction solar cell, including the TCOs on the emitter (left) and BSF (right). Note that for an IBC cell, the horizontal axis of this sketch would be "U shaped", "up" through the emitter and interface, then laterally through the absorber to the BSF region and "down" through the BSF/TCO stack.*

Achieving a low series resistance and thus a high fill factor is one of the major challenges in the development of IBC SHJ devices. Since the contact resistivity between the amorphous or nanocrystalline contact layers and the TCO is a major contributor to the series resistance, optimising these interfaces is crucial in order to obtain high FF values. Within the simplest heterojunction model, the so-called Anderson model, the band line-up at the TCO/Si interface is determined by the work function difference between the two materials. The band line-up, in turn, influences charge carrier transport and thus SHJ cell performance. For example, for the band line-up sketched in **Figure 8**, the TCO/(n)a-Si:H junction in the BSF is almost ideal. However, due to the unfavourable band line-up at the TCO/(p)a-Si:H heterojunction in the emitter contact, a downward band bending, thus a considerable barrier has to be overcome by the holes before then can recombine with electrons supplied by the TCO.

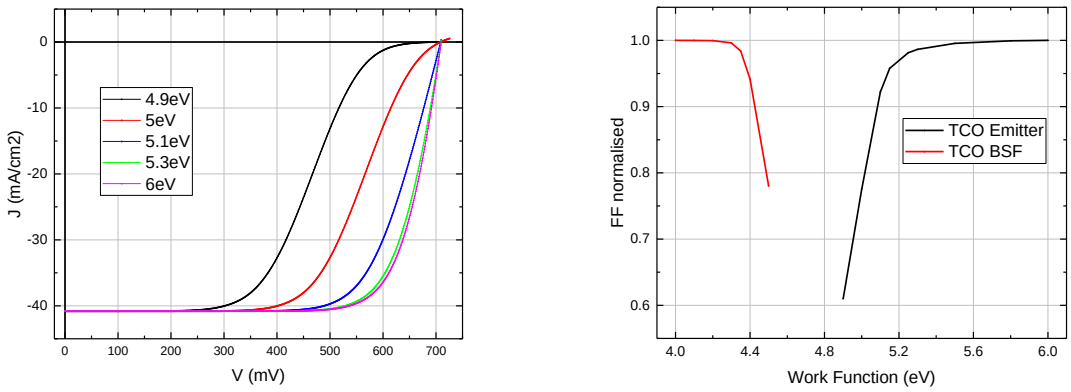

Figure 9: *Simulated dependence of the illuminated I-V curve (left) and the normalised fill factor (right) of IBC-SHJ cells on the work function of the TCOs. For clarity, the I-V curves are shown only for the work function variation of the TCO on the emitter.*

To avoid further complicating the already complex IBC SHJ manufacturing process the same TCO material is often used for both contacts, yielding a situation as presented in Figure 8. For the deliverable, TUD has carried out simulations assuming different TCO work functions both on the emitter and on the BSF contact in order to assess whether the choice of a single TCO, thus a common work function, can be detrimental to IBC SHJ device performance. The simulation results suggest, that there is indeed no common “best value” for the TCO work function that leads to a maximum fill factor: Figure 9 (left) shows the impact of a heavily misaligned Emitter-TCO-contact: S-shaped I-V curves lead to a strong deterioration of the fill factor. This situation occurs for TCOs on the emitter if they have a too low work function (here, below ~5.3 eV). For the TCO on the BSF side, on the other hand, a work function below ~4.3 eV would be desirable. Note, that this reasoning hold quantitatively only if the Anderson model is valid – which is generally not the case. However, the trends seen in the simulation are valid as a description of the experiment. Thus, ideally the two contacts incorporate TCOs with different work functions for an optimal charge carrier extraction (Figure 9, right). These calculations hold for moderately doped a-Si:H films with activation energies of 300 meV and 450 meV for n-aSi and p-aSi, respectively. At these doping levels, too high/too low TCO work functions lead to the formation of Schottky contacts. Thus, the FF degradation becomes apparent when the work function mismatch leads to a Schottky energy barrier that resists a proper carrier collection. This effect is mitigated when the a-Si layers are more highly doped, i.e. feature a lower activation energy. If a higher doping is not feasible/desirable, it might be worth accepting the additional manufacturing effort that comes with providing different TCO materials for each contact in order to minimise the contact resistivity at both interface and thus maximize the fill factor potential.

3 Risks and interconnections

3.1 Risks/problems encountered

The presented simulations are very complex, involving many choices regarding both suitable models and input parameters describing materials properties. As usual in this case, a major challenge is to obtain consistent sets of “microscopic” input parameters (such as optical properties, conductivities, band line-ups etc.) together with a set of “macroscopic” measurements (I-V, quantum efficiency, etc.), ideally including relevant parameter variations. Such data is needed to validate the models and make them predictive, thus useful for further device optimization. It can be challenging to keep experiments and simulations “synchronized”, sec. 2.1.3 is an example: The V_{oc} values of the simulations presented in the first part of that section are rather low because a set of materials properties was used that was consistent, but became superseded quickly by device improvements due to improved (p)a-Si:H film quality. Nevertheless, our models are now well-developed enough to provide realistic estimates of the limits of IBC SHJ cells. Detailed loss analyses for the specific device structures realized by the NextBase partners will be possible as soon as the necessary input data is available.

3.2 Interconnections with other deliverables

In order properly break down the losses of the different solar cell devices of each project partner, accurate modelling of all the different layers is necessary. At the moment **TUD** is gathering the corresponding information from each project partner, to apply the j_{sc} analysis method described in chapter 2.1.2. These results will provide a basis for further improvements in device manufacturing and the upcoming milestone MS6 (predictive simulation model), as well as input for deliverables D8.3 and 8.4.

Furthermore, within WP4 Meyer Burger organises a TLM round robin to evaluate the contact resistivity for all the different layer stacks used by the different project partners. The results should yield valuable input data to increase the simulation accuracy of both the methods presented in chapter 2.1.3 and 2.1.4.

4 Conclusion/summary

Both **TUD** and **HZB** are able to perform 2D-simulation studies using Sentaurus TCAD. **TUD**'s approach of combining the optical and electrical simulation in one accurately modelled structure is very promising as it allows – if properly calibrated – distinguishing between many distinct loss contributions both on the optical as well as on the electrical side. The data necessary to calibrate is being collected.

Already performed simulations at **HZB** can help optimising the rear side geometry of the project partner's devices, although the dimension of certain parameters such as the BSF finger width or the metallization gap are limited by the corresponding manufacturing process. Some quite general conclusions can be drawn from the simulations:

- As long as the passivation properties of different films (emitter / BSF) are at the same level, the ratio of emitter-vs-BSF coverage, and the absolute size of the contacts as defined by this ratio and the unit cell pitch, have a negligible influence on the open circuit voltage
- The fill factor, on the other hand, is very sensitive to the contact size
- due to the high resistivity of a-Si:H, a larger contact is generally beneficial for current collection, which leads to higher FF
- The best pitch is mostly influenced by gap size, minority carrier diffusion length and base resistivity: too large pitches, above the minority carrier diffusion length, lead to current collection losses (drop in photocurrent, j_{sc}) as well as increasing series resistance (FF drop), while the limitations towards small pitches are mostly determined by the structure sizes that can be realized technologically
- For the simulated (realistic) materials properties, the optimum for the technological pitch is of the order of 0.5-1.5 mm.
- The best emitter/BSF ratio is decided by the current collection probability (determined by c-Si bulk and surface properties) as well as the a-Si:H quality (conductivity, contact resistance); with realistic properties of the contact materials it is roughly emitter/BSF = 80/20.
- Both emitter and BSF should be covered as thoroughly as possible by metal contacts; metallization gaps of only 50 µm, which are at the lower end of technologically relevant gap widths, already lead to a slight decrease in solar cell fill factor (a few tenths of a % abs.).
- Regarding optical properties, it could be demonstrated that the front side antireflection/light trapping structures currently available within NextBase are on par with those of the current world record IBC-SHJ cell, which account for ~1 mA/cm² photocurrent loss as compared to the maximally available 43.2 mA/cm² from c-Si wafers, or ~2.3%rel..

5 Literature

[Ingenito2014] A. Ingenito, et al., *ACS Photonics* **1**, 270-278 (2014)

[Ingenito2015] A. Ingenito, et al., *Prog. Photovolt: Res. Appl.* **23**, 1649 - 1659 (2015)

[Richter2012] A. Richter et al., Improved quantitative description of Auger recombination in crystalline silicon. *Physical Review B* **86**, 165202 (2012)

[Yang2016] G. Yang, et al., IBC c-Si solar cells based on ion-implanted poly-silicon passivating contacts. Sol. En. Mat. Sol. Cells 158, 84-90 (2016)

[Yoshikawa2017] K. Yoshikawa et al., Silicon heterojunction solar cell with interdigitated back contacts for a photoconversion efficiency over 26%. Nature Energy **2**, 17032 (2017)

[Procel2017] P. Procel et al., Opto-electrical modelling and optimization study of a novel IBC c-Si solar cell. Progress in Photovoltaics: Research and Applications. 25, 6 452-469 (2017)